Closing the gap between galvanic and inductive methods: EEMverter, a new 1D/2D/3D inversion tool for Electric and Electromagnetic data with focus on Induced Polarization

Gianluca Fiandaca*
The EEM Team for Hydro & eXploration,
Dep. of Earth Sciences A. Desio,
Università degli Studi di Milano,
Via Botticelli 23, Milano (Italy)
gianluca.fiandaca@unimi.it

Bo Zhang
Institute of Earth exploration,
Science and Technology,
Jilin University,
Changchun (China)
em_zhangbo@163.com

Jian Chen
The EEM Team for Hydro & eXploration
Dep. of Earth Sciences A. Desio,
Università degli Studi di Milano,
Via Botticelli 23, Milano (Italy)
jian.chen@unimi.it

Alessandro Signora
The EEM Team for Hydro & eXploration,
Dep. of Earth Sciences A. Desio,
Università degli Studi di Milano,
Via Botticelli 23, Milano (Italy)
alessandro.signora@unimi.it

Francesco Dauti
The EEM Team for Hydro & eXploration,
Dep. of Earth Sciences A. Desio,
Università degli Studi di Milano,
Via Botticelli 23, Milano (Italy)
francesco.dauti@unimi.it

Stefano Galli
The EEM Team for Hydro & eXploration
Dep. of Earth Sciences A. Desio,
Università degli Studi di Milano,
Via Botticelli 23, Milano (Italy)
stefano.galli@unimi.it

Nicole Anna Lidia Sullivan
The EEM Team for Hydro & eXploration,
Dep. of Earth Sciences A. Desio,
Università degli Studi di Milano,
Via Botticelli 23, Milano (Italy)
nicole.sullivan@unimi.it

Arcangela Bollino
The EEM Team for Hydro & eXploration,
Dep. of Earth Sciences A. Desio,
Università degli Studi di Milano,
Via Botticelli 23, Milano (Italy)
arcangela.bollino@unimi.it

Andrea Viezzoli
EMergo srl,

Via XX Settembre 12, Cascina, (Pisa, Italy)
andrea.viezzoli@em-ergo.it

SUMMARY

The interest on Induced Polarization (IP) in AEM data (AIP) has significantly increased in recent years, both within the research community and in the industry. However, the inversion of AIP data is particularly ill-posed, especially when spectral modelling, such as Cole-Cole modelling, is used. Furthermore, the comparison of AIP and galvanic ground IP inversion models is hindered by the fact that the IP effect is usually modelled differently in the inductive and galvanic computations.

In this study we present a new inversion software, EEMverter, which has been developed to model IP in electric and electromagnetic (EM) data within the same inversion framework. In particular, three specific goals have been identified within EEMverter's development: i) to allow multiple inversion cycles that mix, sequentially or simultaneously, 1D, 2D and 3D forward modelling, for diminishing the inversion burden; ii) to allow the joint inversion of AIP, ground EM-IP and ground galvanic IP data; iii) to allow time-lapse inversions of AIP, EM and galvanic IP data.

EEMverter has been tested on several AEM and AIP surveys, also in conjunction with ground EM and ground galvanic IP data in joint inversion. In this study, the inversion of the VTEM AIP survey over the Valen Cu-Ni deposit is presented, highlighting the improvements in model resolution when compared to standard inversion approaches.

Key words: Induced Polarization, Joint Inversion, 1D, 2D, 3D, galvanic

INTRODUCTION

The induced polarization (IP) phenomenon in airborne electromagnetic AEM data (AIP) presents a challenge to exploration in many parts of the world. It is a well-known phenomenon since Smith and Klein (1996) first demonstrated the presence of IP effects, which have been further discussed by several authors (e.g., Marchant *et al.*, 2014; Macnae, 2016; Viezzoli *et al.*, 2017). IP-affected AEM data are often interpreted in terms of the Cole-Cole model (e.g., Marchant et al., 2014; Viezzoli *et al.*, 2017; Lin *et al.*, 2019), but the inversion problem is particularly ill-posed: for a 1D inversion of a single sounding four parameters have to be retrieved for each model layer. Furthermore, AIP and ground IP modelling are usually carried out in different inversion frameworks, making difficult a direct comparison of the results. In this study we present a novel inversion software, EEMverter, specifically developed to model electric and electromagnetic data taking into account the IP phenomenon. Three distinctive features have been implemented in EEMverter: i) 1D, 2D and 3D forward modelling can be mixed sequentially or simultaneously in the iterative process within multiple inversion cycles, for diminishing the computational burden; ii) the joint inversion of AIP, ground EM-IP and ground galvanic IP data is fully supported with a common IP parameterization; iii) time-lapse inversions of AIP, EM and galvanic IP data is possible with both sequential and simultaneous approaches. In the following, the implementation of EEMverter is described, with examples of synthetic and field inversion results.

METHOD

In EEMverter the inversion parameters are defined on model meshes which do not coincide with the forward meshes used for data modelling: the link between model and forward meshes is obtained interpolating the model mesh parameters into the forward mesh discretization, as done for 1D AEM in Christensen et al. (2017), in 3D galvanic IP in Madsen et al.

(2020) and in 3D EM in Zhang et al. (2021), Engebretsen et al. (2022) and Xiao et al. (2022a). This spatial decoupling allows for defining the model parameters, e.g. the Cole-Cole ones, on several model meshes, for instance one for each inversion parameter. In this way, it is possible to define the spectral parameters, like the time constant and the frequency exponent in the Cole-Cole model, on meshes coarser than the resistivity and chargeability ones, vertically and/or horizontally, with a significant improvement in parameter resolution.

For each dataset of the inversion process, a distinct forward mesh is defined. The interpolation from the model parameters $\boldsymbol{M}$ defined on the model mesh nodes into the values $\boldsymbol{m_i}$ at the subdivisions of the i[th] forward mesh is expressed through a matrix multiplication, in which the matrix $\boldsymbol{F_i}$ holds the weights of the interpolation, which depends only on the distances between model mesh nodes and the subdivisions of the i[th] forward mesh:

$$\boldsymbol{m_i} = f_i(\boldsymbol{M}) = \boldsymbol{F_i} \cdot \boldsymbol{M} \qquad (1)$$

In EEMverter 1D, 2D and 3D forward & Jacobian computations have been implemented. In particular, Transient EM data are modelled in 1D following Effersø et al. (1999); in 3D the forward solution is carried out in frequency domain, with the finite element method, both with tetrahedral elements or with the octree approach, similarly to what has been done with the time-stepping time-domain approach in Zhang et al. (2021) and Xiao et al. (2022a). The finite element approach is used also for frequency-domain galvanic computations in 2D (Fiandaca et al., 2013) and 3D (Madsen et al., 2020). The transformation to time-domain is obtained through a fast Hankel transformation (as in Effersø et al., 1999) for both the forward response and the Jacobian. In particular, the time-domain Jacobian in the i[th] forward mesh is computed as:

$$\boldsymbol{J_{m_i,TD}} = \boldsymbol{A} \cdot \boldsymbol{T} \cdot \boldsymbol{J_{m_i,FD}} \qquad (2)$$

Where the matrix $\boldsymbol{T}$ holds the Hankel coefficients, the matrix $\boldsymbol{A}$ implements the effects of current waveform, gate integration and filters and the frequency-domain Jacobian $\boldsymbol{J_{m_i,FD}}$ is calculated in 1D through finite difference and in 2D/3D using the adjoint method and the chain rule as in Fiandaca et al. (2013) and Madsen et al. (2020):

$$\boldsymbol{J_{m_i,FD}} = \boldsymbol{J_{\sigma^*,i}} \cdot \frac{\partial \sigma^*}{\partial m_i} \qquad (3)$$

where $\boldsymbol{J_{\sigma^*,i}}$ is the Jacobian of the i[th] forward mesh with respect to the complex conductivity $\boldsymbol{\sigma^*}$ and $\frac{\partial \sigma^*}{\partial m_i}$ is the partial derivative of the complex conductivity versus the model parameters. This approach, contrary to the time stepping approach, allows to use any parameterization of the IP phenomenon in the inversion. Finally, the Jacobian of the model space $\boldsymbol{J_M}$ is computed summing the contributions of all forward meshes up (Christensen et al., 2017; Madsen et al., 2020, Zhang et al., 2021), using the domain decomposition with a forward mesh for each sounding in 3D EM computations (Cox et al., 2010; Zhang et al., 2021):

$$\boldsymbol{J_M} = \sum_i \boldsymbol{J_{m_i}} \cdot \boldsymbol{F_i}^T \qquad (4)$$

The total Jacobian is used for computing the inversion model in a Levenberg-Marquardt linearized approach as follows:

$$\boldsymbol{M_{n+1,j}} = \boldsymbol{M_{n,j}} + \left[\boldsymbol{J_{M,j}}^T \boldsymbol{C_d}^{-1} \boldsymbol{J_{M,i}} + \boldsymbol{R}^T \boldsymbol{C_{R,j}}^{-1} \boldsymbol{R_j} + \lambda \boldsymbol{I}\right]^{-1} \cdot \left[\boldsymbol{J_{M,j}}^T \boldsymbol{C_d}^{-1} \cdot \left(\boldsymbol{d} - \boldsymbol{f_{n,j}}\right) + \boldsymbol{R}^T \boldsymbol{C_{R,j}}^{-1} \boldsymbol{R_j} \cdot \boldsymbol{M_{n,j}}\right] \qquad (5)$$

In equation (5) the subscript j indicates that the inversion process can be split in several inversion cycles: in each cycle j it is possible to change the forward computation for each dataset (e.g. from 1D to 3D), as well as to insert/remove data/constraints from the objective function. Figure (1) shows the 3-cycle inversion scheme for AIP inversion, in which the parameters of the Maximum Phase Angle (MPA) Cole-Cole reparameterization (Fiandaca et al., 2018) are defined in two distinct model meshes: the resistivity $\boldsymbol{\rho}$ and the phase $\boldsymbol{\varphi}$ vary both horizontally and vertically (Figure 1a), but the time constant $\boldsymbol{\tau}$ and the frequency exponent $\boldsymbol{C}$ vary only horizontally (Figure 1b), for increasing the sensitivity of the spectral parameters.

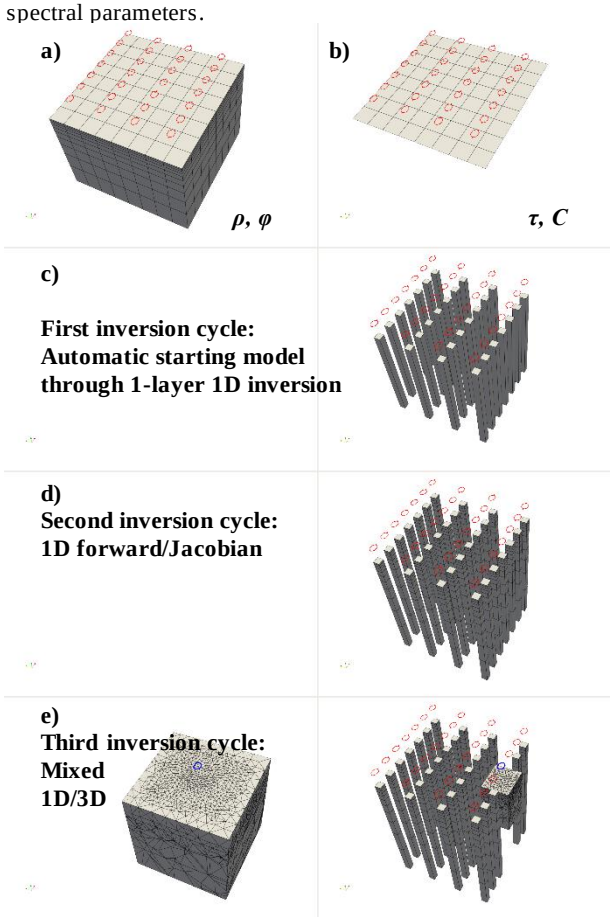

Figure 1. EEMverter multi-cycle inversion scheme for 3D AEM inversion with Induced polarization. a) Model mesh for resistivity ρ and phase φ, with depth variability, with red polygons representing AEM frames. b) Model mesh for relaxation time τ and frequency exponent C, without depth variability. c) First inversion cycle for computation of automatic starting model, with 1D forward meshes (grey bars) composed by only one layer. d) Second inversion cycle with 1D forward/Jacobian computations, with vertical discretization of the 1D forward meshes (grey bars). e) Third inversion cycle with mixed dimensionality of the forward/Jacobian meshes: 1D for the soundings with red frames and 3D for the soundings with blue frames (left: 3D Mesh; right: subset of the 3D mesh and 1D meshes)

The 3-cycle inversion comprises: i) a first cycle which finds the best starting model without vertical variability of the parameters, through the use of a single-layer 1D forward mesh (Figure 1c); ii) a second cycle with 1D forward/Jacobian computations; iii) a third cycle that switches to 3D computations the soundings in area with strong contrasts in electrical properties.

Figure 2 presents the model and forward meshes for a joint inversion, in which 1D AEM and 1D ground EM computations are combined with 2D galvanic computations.

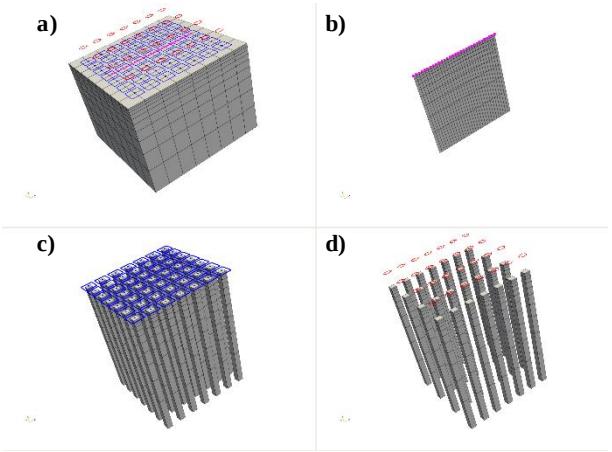

Figure 2. EEMverter multi-mesh inversion scheme for Joint inversion of inductive and galvanic data. a) Model mesh and data positions: red polygons for AEM frames; blue squares for ground TEM frames; magenta line for galvanic 2D profile. b) Galvanic 2D forward mesh. c) Ground TEM frames (blue squares) and corresponding 1D soundings (grey bars). d) AEM frames (red polygons) and corresponding 1D soundings (grey bars).

Figure (3) presents the time-lapse approach of EEMverter, in which all the models of all the time steps can be inverted at once, without the need of relocating the model meshes when the positions of the acquisitions vary among the time steps, as in Xiao et al. (2022b).

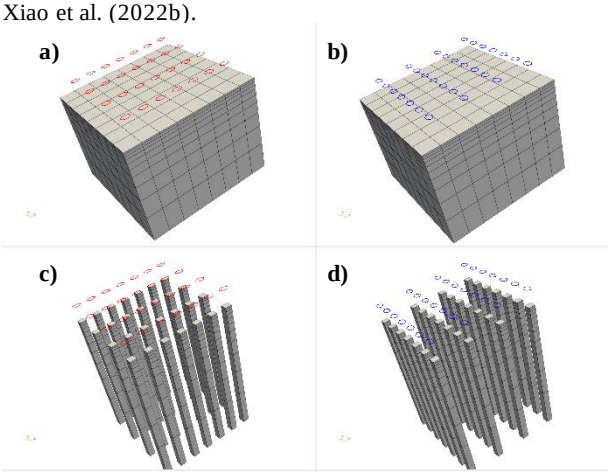

Figure 3. EEMverter multi-mesh inversion scheme for Time-Lapse inversion. a) Model mesh corresponding to the first Time-lapse acquisition (red polygons). Model mesh corresponding to the second Time-lapse acquisition (blue polygons), identical to the first model mesh despite of the different sounding positions. c) Forward meshes (grey bars) of the first acquisition (red frames). d) Forward meshes (grey bars) of the second acquisition (blue frames).

RESULTS

The joint inversion of AEM, ground EM and galvanic IP data through EEMverter is presented in Dauti et al. (2023) in applications related to mineral exploration and in Signora et al. (2023) for the characterization of the HydroGeosITe, the Italian reference and calibration site for hydrogeophysical methods under development in Brescia, Italy.

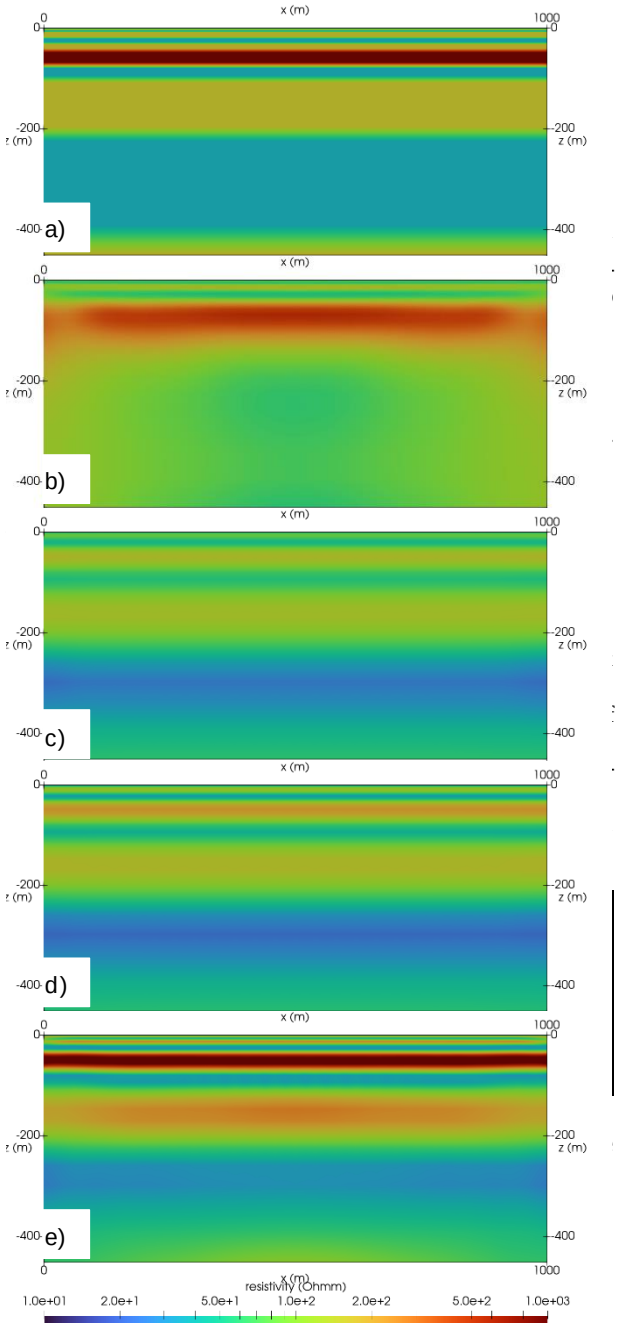

Figure 4. Synthetic model and inversion results. a) resistivity section of a MPA IP simulation of electrical properties; b) inversion model of DCIP data; c) inversion model of AEM+ground EM data; d) inversion model of AEM+ground EM+tTEM data; e) joint inversion of all inductive and galvanic data.

In both cases a unique inversion model in terms of MPA parameterization is able to describe both inductive and full-decay galvanic data, with data misfits very similar to the ones

obtained with independent inversions, in contrast to the findings of Christiansen et al. (2007). Figure 4 presents the resistivity section of a synthetic model that mimics the electrical properties (both conduction and polarization) of sand, clay and consolidated formations, based on the petrophysical relations described in Weller et al. (2015), together with the inversion model of inductive and galvanic data. In particular, four different inversion results are presented: direct current and full-decay induced polarization (DCIP) galvanic data, with 10 m electrode spacing and 2D gradient sequence; AEM + ground EM data, with sounding distance of 40 m; AEM+ground EM + tTEM data (Auken et al., 2019), with tTEM soundings every 10 m; all data together in a joint inversion scheme.

The joint inversion presents much better resolution capability, with the inductive and galvanic data complementing each other in resolving both conductive and resistive layers. The same kind of improvement is found in Signora et al. (2023) with field data. Another example of joint inversion of AEM and galvanic VES data in EEMverter, without IP modelling but with integration with resistivity logs is presented in Galli et al. (2023), where the asymmetric minimum support norm (Fiandaca et al., 2015) is used for an automated rejection of conflicting borehole information. A similar approach is implemented in EEMverter also for automatic processing of AEM data (2021).

The second EEMverter inversion presented in this study is the AIP inversion of four lines of the VTEM survey carried out on the Valen Cu-Ni deposit, in South Australia, consisting of 1108 soundings, with the approach presented in figure (1), but without the final 3D inversion cycle, which will be presented at the conference.

Table 1 presents a comparison of the sensitivities of the four Cole-Cole parameters, in terms of maximum elements of the $\boldsymbol{J_P}^T \boldsymbol{C_d}^{-1} \boldsymbol{J_P}$ matrix, for two cases: 1) no vertical variability for τ and C (i.e. τ and C defined on the mesh of Figure (1b); 2) vertical variability for τ and C (i.e. τ and C defined on the mesh of Figure (1a). Coarsening the spatial discretization of τ and C, allowing no vertical variability, causes an increase in their sensitivity more than ten-fold, with a significant improvement in resolution and decrease in correlations among parameters.

Figure 5 shows the inversion model of the four MPA parameters of the Valen data, while Figure 6 presents the fit of one line, plotted in EEMstudio (Sullivan et al., 2023). Very good fit is reached in the inversion, with the IP modelling decreasing the overall data misfit of more than 20%, when compared to the resistivity-only inversion.

Table 1. Maximum element of the matrix $J_P{}^T C_d{}^{-1} J_P$, for the first iteration of the Valen inversion, without vertical variability for τ and C (Figure 1b) and with vertical variability (Figure 1a).

parameter	Max $J_P{}^T C_d{}^{-1} J_P$ value, τ and C **without** vertical variability	Max $J_P{}^T C_d{}^{-1} J_P$ value, τ and C **with** vertical variability
ρ	3.5E+03	3.5E+03
φ_{max}	2.1E+02	2.1E+02
τ	6.5E+01	5.9E+00
C	3.2E+02	1.7E+01

CONCLUSIONS

We presented EEMverter, a novel inversion software for electric and electromagnetic data with focus on induced polarization. Three distinctive features have been implemented in EEMverter: i) 1D, 2D and 3D forward modelling can be mixed sequentially or simultaneously in the iterative process within multiple inversion cycles, for diminishing the computational burden; ii) the joint inversion of AIP, ground EM-IP and ground galvanic IP data is fully supported with a common IP parameterization; iii) time-lapse inversions of AIP, EM and galvanic IP data is possible with both sequential and simultaneous approaches.

We tested EEMverter on several synthetic and field data sets, with AIP inversions alone and in joint inversion between: i) different AEM systems, ii) AEM and ground based EM data and iii) AEM, ground EM and galvanic full-decay DCIP data. In particular, the synthetic example of joint inversion of AEM, ground EM and DCIP data presented in this study shows a significant improvement in spatial resolution, with inductive and galvanic data complementing each other in an excellent retrieval of both conductive and resistive anomalies. The field example of the AIP inversion of the VTEM data acquired over the Valen Cu-Ni deposit shows a significant improvement in data fit in comparison with the resistivity-only inversion. Furthermore, the definition of the spectral Cole-Cole parameters in a separate inversion mesh without vertical variability allows to enhance significantly their resolution. We believe that EEMverter, with its common inversion environment for the IP inversion of inductive and galvanic data will help in closing the gap between electric and electromagnetic data in AEM applications.

ACKNOWLEDGMENTS

This study has been partially carried out within the Horizon Europe project SEMACRET. Thanks to CSIRO and Tim Munday for providing the AEM Valen data.

REFERENCES

Auken E., Foged N., Larsen J.J., Trøllund Lassen K.V., Maurya P.K., Dath S.M., Eiskjær T.T (2019). tTEM — A towed transient electromagnetic system for detailed 3D imaging of the top 70 m of the subsurface. *Geophysics, 84 (1), E13-E22.*

Christensen, N. K., Ferre, T. P. A., Fiandaca, G., & Christensen, S. (2017). Voxel inversion of airborne electromagnetic data for improved groundwater model construction and prediction accuracy. *Hydrology and Earth System Sciences*, *21*(2), 1321-1337.

Christiansen, A. V., Auken, E., Foged, N., & Sørensen, K. I. (2007). Mutually and laterally constrained inversion of CVES and TEM data: a case study. *Near Surface Geophysics*, *5*(2), 115-123.

Cox, L. H., Wilson, G. A., & Zhdanov, M. S. (2010). 3D inversion of airborne electromagnetic data using a moving footprint. *Exploration Geophysics*, *41*(4), 250-259.

Dauti, F., Viezzoli, A., Fiandaca, G. (2023). Joint Inversions of AEM modelling AIP effects: Helicopter-borne, Ground IP and Fixed-Wing systems. *AEM2023 - 8th International Airborne*

Electromagnetics Workshop, 3-7 September 2023, Fitzroy Island, QLD, Australia.

Effersø, F., Auken, E., & Sørensen, K. I. (1999). Inversion of band-limited TEM responses. *Geophysical Prospecting*, 47(4), 551-564.

Engebretsen, K. W., Zhang, B., Fiandaca, G., Madsen, L. M., Auken, E., & Christiansen, A. V. (2022). Accelerated 2.5-D inversion of airborne transient electromagnetic data using reduced 3-D meshing. *Geophysical Journal International*, *230*(1), 643-653.

Fiandaca, G., Auken, E., Christiansen, A. V., & Gazoty, A. (2012). Time-domain-induced polarization: Full-decay forward modeling and 1D laterally constrained inversion of Cole-Cole parameters. *Geophysics*, *77*(3), E213-E225.

Fiandaca, G., Ramm, J., Binley, A., Gazoty, A., Christiansen, A. V., & Auken, E. (2013). Resolving spectral information from time domain induced polarization data through 2-D inversion. *Geophysical Journal International*, *192*(2), 631-646.

Fiandaca, G., Doetsch, J., Vignoli, G., & Auken, E. (2015). Generalized focusing of time-lapse changes with applications to direct current and time-domain induced polarization inversions. *Geophysical Journal International*, *203*(2), 1101-1112.

Fiandaca, G., Madsen, L. M., & Maurya, P. K. (2018). Re-parameterisations of the Cole–Cole model for improved spectral inversion of induced polarization data. *Near Surface Geophysics*, *16*(4), 385-399.

Fiandaca, G., Viezzoli, A. (2021). Inversion of Airborne IP data with a multi-mesh approach for parameter definition. *Australasian Exploration Geoscience Conference AEGC2021, 13-17 September 2021, Virtual Conference.*

Fiandaca, G. (2021). Inversion-based automatic processing of AEM data. *Australasian Exploration Geoscience Conference AEGC2021, 13-17 September 2021, Virtual Conference.*

Galli, S., Shaars, F., Smits, F., Borst, L., Rapiti, A., Fiandaca G. (2023). Automated integration of AEM data, VES and borehole logs. *AEM2023 - 8th International Airborne Electromagnetics Workshop, 3-7 September 2023, Fitzroy Island, QLD, Australia*.

Lin, C., Fiandaca, G., Auken, E., Couto, M. A., & Christiansen, A. V. (2019). A discussion of 2D induced polarization effects in airborne electromagnetic and inversion with a robust 1D laterally constrained inversion scheme. *Geophysics*, 84(2), E75-E88.

Haber, E., Oldenburg, D. W., & Shekhtman, R. (2007). Inversion of time domain three-dimensional electromagnetic data. *Geophysical Journal International*, *171*(2), 550-564.

Kang, S., Oldenburg, D. W., & Heagy, L. J. (2020). Detecting induced polarisation effects in time-domain data: a modelling study using stretched exponentials. *Exploration Geophysics*, *51*(1), 122-133.

Lin, C., Fiandaca, G., Auken, E., Couto, M. A., & Christiansen, A. V. (2019). A discussion of 2D induced polarization effects in airborne electromagnetic and inversion with a robust 1D laterally constrained inversion scheme. Geophysics, 84(2), E75-E88.

Marchant, D., E. Haber, and D. Oldenburg, 2014, Three-dimensional modeling of IP effects in time-domain electromagnetic data: Geophysics, 79, no. 6, E303–E314, doi: 10.1190/geo2014-0060.1.

Madsen, L. M., Fiandaca, G., & Auken, E. (2020). 3-D time-domain spectral inversion of resistivity and full-decay induced polarization data—full solution of Poisson's equation and modelling of the current waveform. *Geophysical Journal International*, *223*(3), 2101-2116.

Signora, A., Galli, S., Gisolo, M., Fiandaca, G. (2023). The HydroGeosITe for AEM mapping: characterization through joint inversion of AEM, ground EM and DCIP data. *AEM2023 - 8th International Airborne Electromagnetics Workshop, 3-7 September 2023, Fitzroy Island, QLD, Australia*.

Sullivan, N.A.L., Viezzoli, A., Fiandaca, G. (2023). EEMstudio: an open-source freeware QGIS plugin for processing, modelling and inversion of electric and electromagnetic data. *AEM2023 - 8th International Airborne Electromagnetics Workshop, 3-7 September 2023, Fitzroy Island, QLD, Australia*.

Viezzoli, A., V. Kaminski, and G. Fiandaca, 2017, Modeling induced polarization effects in helicopter time domain electromagnetic data: Synthetic case studies. *Geophysics*, 82, no. 2, E31–E50.

Weller, A., Slater, L., Binley, A., Nordsiek, S., & Xu, S. (2015). Permeability prediction based on induced polarization: Insights from measurements on sandstone and unconsolidated samples spanning a wide permeability range. *Geophysics*, *80*(2), D161-D173.

Xiao, L., Fiandaca, G., Zhang, B., Auken, E., & Christiansen, A. V. (2022a). Fast 2.5 D and 3D inversion of transient electromagnetic surveys using the octree-based finite-element method. *Geophysics*, *87*(4), E267-E277.

Xiao, L., Fiandaca, G., Maurya, P. K., Christiansen, A. V., & Lévy, L. (2022b). Three-dimensional time-lapse inversion of transient electromagnetic data, with application at an Icelandic geothermal site. *Geophysical Journal International*, *231*(1), 584-596.

Zhang, B., Engebretsen, K. W., Fiandaca, G., Cai, H., & Auken, E. (2021). 3D inversion of time-domain electromagnetic data using finite elements and a triple mesh formulation. *Geophysics*, *86*(3), E257-E267.

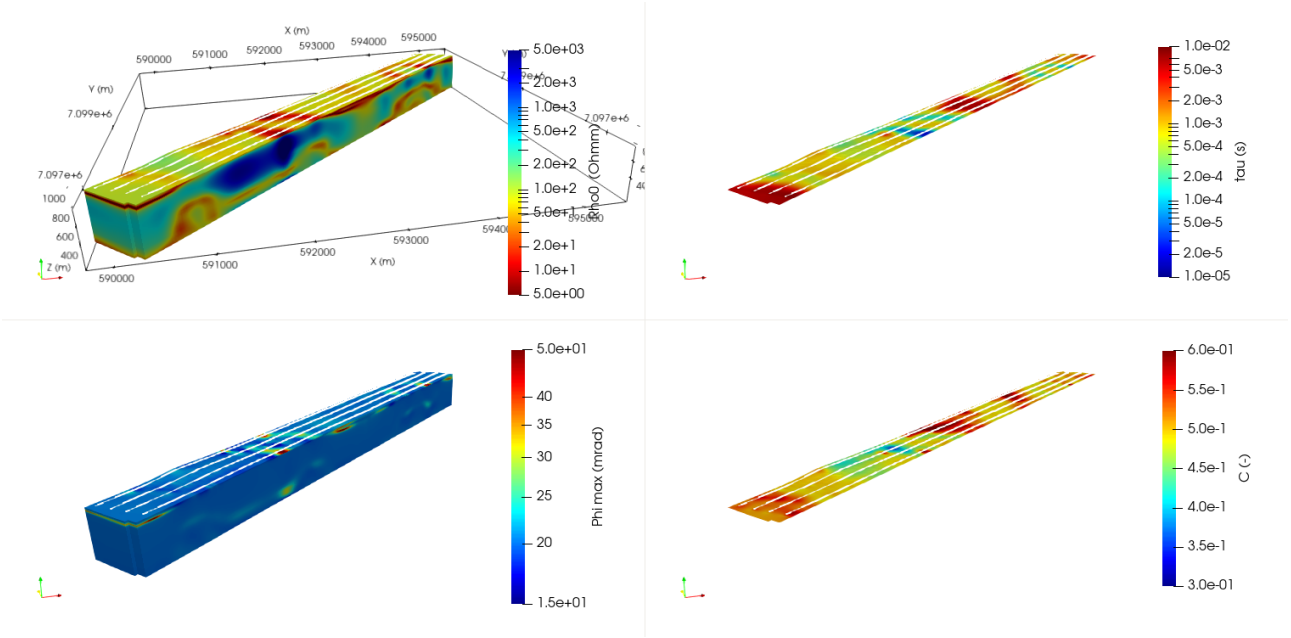

Figure 5. EEMverter inversion model of the Valen VTEM survey. Top left – resistivity model; Bottom left – chargeability (maximum phase) model; Top right –model of the time constant tau; Bottom right – model of the spectral exponent C. White lines represent the acquisition lines.

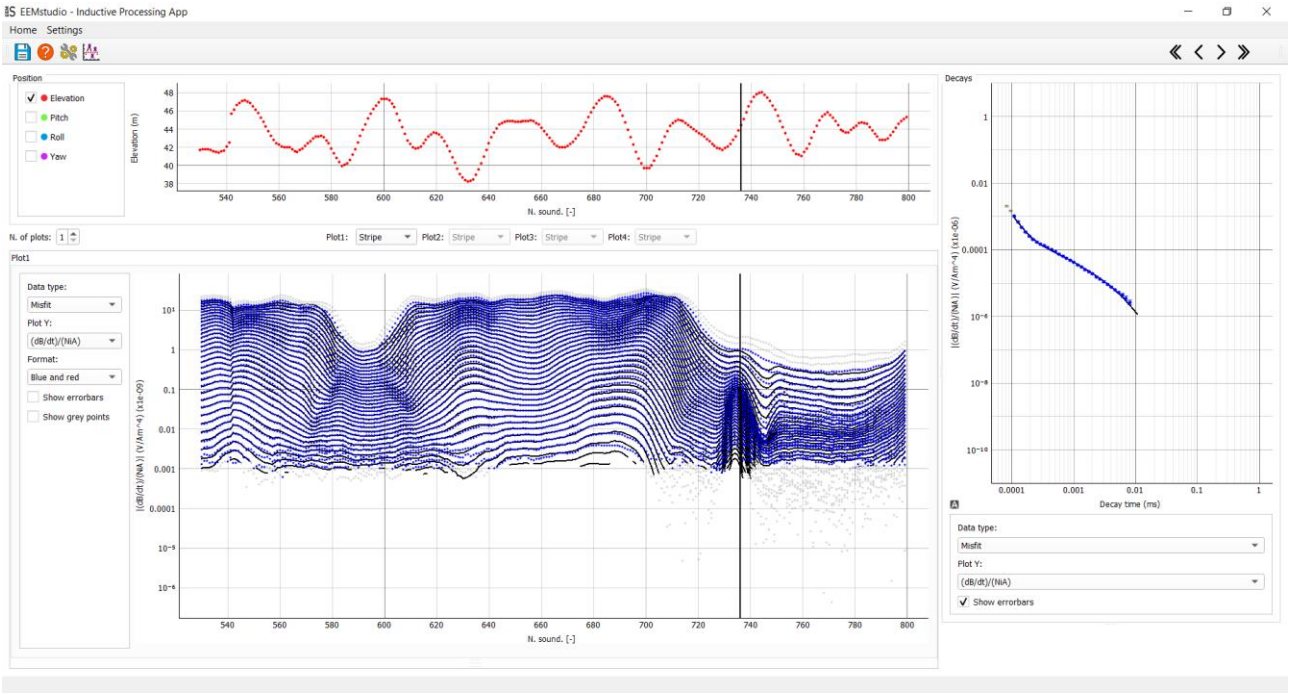

Figure 6. Fit of EEMverter inversion in correspondance to the strongest conductivity anomaly displayed through EEMstudio (Sullivan et al., 2023). Top section: flight altitude; bottom section: data (blue markers) and gate-by-gate fit (black lines); right panel: exemplary decay in correspondance to the vertical black line along the data stripe.